10-1987

Gamma-ray observations of the Crab Region using a coded-aperture telescope

Mark L. McConnell
University of New Hampshire - Main Campus, mark.mcconnell@unh.edu

P. P. Dunphy
University of New Hampshire - Main Campus

D J. Forrest
University of New Hampshire - Main Campus

E. L. Chupp
University of New Hampshire - Main Campus

A Owens
University of Leicester

Recommended Citation
M.L. McConnell, P.P. Dunphy, D.J. Forrest, E.L. Chupp, and A. Owens, GAMMA-RAY OBSERVATIONS OF THE CRAB REGION USING A CODED-APERTURE TELESCOPE, 1987, Ap. J., 321, 543.

THE ASTROPHYSICAL JOURNAL, 321:543–552, 1987 October 1

GAMMA-RAY OBSERVATIONS OF THE CRAB REGION USING A CODED-APERTURE TELESCOPE

M. L. MCCONNELL, P. P. DUNPHY, D. J. FORREST, E. L. CHUPP, AND A. OWENS
Physics Department, University of New Hampshire
Received 1986 December 15; accepted 1987 February 26

ABSTRACT

The region of the Galactic anticenter, including the Crab Nebula, was observed during a balloon flight of a new γ-ray telescope employing the coded-aperture imaging technique. The observations were made over Palestine, Texas, on 1984 October 2 and covered the energy range of 160 keV to 9.3 MeV with an imaging field of view of 15°.2 by 22°.8. The instrument's imaging response to the Crab was found to be well represented by a Gaussian function with a full width at half-maximum (FWHM) of 4°.8. The centroid of the measured response is located with an uncertainty of $\pm 12'$ (68% confidence level). The derived spectrum of the Crab, incident on the top of the atmosphere, is consistent with a single power-law spectrum of the form $AE(\mathrm{MeV})^{-\alpha}$ photons $\mathrm{cm}^{-2}\ \mathrm{s}^{-1}\ \mathrm{MeV}^{-1}$, where $A = (5.1^{+2.4}_{-1.6}) \times 10^{-3}$ and $\alpha = 1.88 \pm 0.23$. We place 3 σ upper limits of 3.2×10^{-3} and 1.9×10^{-3} photons $\mathrm{cm}^{-2}\ \mathrm{s}^{-1}$ on line features from the Crab at energies of 405 keV and 1050 keV, respectively. The imaging nature of the experiment, coupled with its large field of view, allow us to derive upper limits to the flux from the nearby binary X-ray source A0535+26 and to the diffuse Galactic emission in the Galactic anticenter region. The results presented here clearly demonstrate the ability of the coded-aperture technique to spatially image γ-ray photons over a large field of view, to determine point source locations (in two dimensions simultaneously) with a high degree of precision, and simultaneously determine the source photon spectra.

Subject headings: gamma rays: general — nebulae: Crab Nebula

I. INTRODUCTION

The observation of cosmic γ-rays in the nuclear transition region (from $\sim$100 keV to 10 MeV) provides a unique method for studying the interactions of particles and fields which are predicted to occur at many astrophysical sites (see Ramaty and Lingenfelter [1982] and references therein). Potential sources include supernovae, novae, neutron stars, and black holes. Spatially extended emission is also expected to arise as a consequence of the interactions of cosmic rays with the ambient interstellar medium. Historically, however, this energy region has been plagued with experimental difficulties. Low source fluxes and high instrumental backgrounds result in poor detection sensitivity. Furthermore, the collimation techniques which have been widely used in the past allow for only very limited spatial resolution. The desire to measure precise source locations as well as to map broad diffuse emission dictates the need for some type of image-forming process. Unfortunately, the penetrating nature of γ-radiation renders traditional imaging techniques, such as optical imaging, ineffective. One viable means for imaging high-energy photons, based on the idea of a pinhole camera, is known as coded-aperture imaging. This method was originally suggested by Dicke (1968) and, independently, by Ables (1968).

In recent years, there have been a number of successful laboratory tests of the coded-aperture concept covering a wide range of X-ray and γ-ray energies (e.g., Cook *et al.* 1983; McConnell *et al.* 1982; Jenkins *et al.* 1984). These tests were conducted with the ultimate goal of imaging celestial sources of radiation. A few experimenters have used this technique to successfully measure celestial X-ray emission at energies below 30 keV (e.g., Proctor, Skinner, and Willmore 1978; Skinner *et al.* 1986). Here we present the first results of its astronomical application at energies above 160 keV. In particular, we report imaging observations of the Galactic anticenter region. This region, which includes the Crab Nebula/pulsar, is well suited for evaluating the inflight properties of a coded-aperture imaging system.

There have been a large number of γ-ray observations made of the Crab region over the past 20 years. Although the measurements of the Crab spectrum are generally consistent with a power-law source spectrum, there have been occasional reports of line emission, most notably at energies of $\sim$78 keV, $\sim$400 keV, and 1049.8 keV (Leventhal, MacCallum, and Watts 1977; Manchanda *et al.* 1982; Ling *et al.* 1979; Yoshimori *et al.* 1979; Strickman, Kurfess, and Johnson 1982; Ayre *et al.* 1983; Owens, Myers, and Thompson 1985; Watanabe 1985). In addition, some observers have reported emission between 1 and 10 MeV which appears to lie well above the power-law extrapolations from both low-energy and high-energy measurements (Baker *et al.* 1973; Gruber and Ling 1977). Due to the potential significance of nuclear line emissions, it is important to obtain confirming evidence for these measurements. The observations presented here allow us to test for the presence of such spectral features. In addition, the imaging nature of the observation enables us to rule out any potential contamination of the Crab photon spectrum by the nearby X-ray source A0535+26 as well as to test for the presence of the anticenter diffuse emission reported by Graser and Schönfelder (1982).

The observations presented in this paper represent the first results obtained from a balloon flight of the University of New Hampshire (UNH) Directional Gamma-Ray Telescope (DGT), an experiment which employs the coded-aperture technique to image celestial γ-radiation between 160 keV and 9.3 MeV. In § II we present an overview of the coded-aperture imaging technique. A description of the DGT is provided in § III, fol-

lowed by a summary of the relevant observations in § IV. Section V details the analysis procedure and the observational results on the Crab region. Finally, a discussion of the scientific results is presented in § VI.

II. CODED-APERTURE TECHNIQUE

A coded-aperture, or "multipinhole," telescope consists of a coded mask situated in front of, and parallel to, a position-sensitive photon detection plane. The mask consists of a combination of open (i.e., transparent) and closed (i.e., opaque) elements. Each open element of the mask acts as an independent pinhole camera to cast an image of the source distribution onto the detection plane. The resulting pattern on the detection plane consists of a large number of overlapping images of the source and therefore bears little resemblance to the actual source distribution. An image of the source may then be recreated using some appropriate reconstruction procedure. This approach retains the angular resolution afforded by a pinhole camera, while increasing the sensitivity to a level commensurate with the needs of the γ-ray astronomer. The angular resolution of the instrument is, in general, determined by the size of the basic aperture opening (or "pinhole"), the mask-detection plane separation, and the accuracy to which the photon interaction point can be determined. It should be noted that this method is applicable for photons of any wavelength, as long as diffraction effects can be ignored.

In order to describe the imaging process, let A be the aperture transmission function (equal to 1 for a perfectly transparent element and 0 for a perfectly opaque element) and S be the distribution of the source emission (i.e., the source being imaged). The response of the photon detection plane, in terms of the spatial distribution of detected photons, will be represented by P. Finally, B represents the spatial distribution of the (unmodulated) background within the photon detection plane. The imaging process can then be described by a correlation of the source distribution (S) and the aperture transmission function (A),

$$P = S * A + B , \tag{1}$$

where $*$ is the correlation operator. These functions may also be represented in terms of discrete array elements. In this case, each element of the source distribution function (S) corresponds to an image-resolution element or pixel, which is equivalent to the area contained within the solid angle subtended by a single mask element as seen from the detection plane. For a source at infinity, each element of both the detector response (P) and the detector background (B) corresponds to an area on the detection plane which is equivalent to the size of a mask element. In terms of these discrete elements, equation (1) can be written as

$$P(k, l) = \sum_{i=1}^{I} \sum_{j=1}^{J} S(i, j)A(i + k, j + l) + B(k, l) , \tag{2}$$

where $I \times J$ is equal to the total number of elements in the detection plane.

Let us now assume that the reconstructed image, S′, can be obtained by correlating the detector response (P) with some suitably chosen postprocessing function (G). This can be expressed mathematically as

$$S' = \mathrm{P} * G = RS * (A * G) + B * G , \tag{3}$$

where R is the reflection operator [i.e., $Rf(x) = f(-x)$]. Note that for a point source, in which case S is a δ-function, the first term reduces to $A * G$. The quantity $A * G$ is therefore equivalent to the point spread function (PSF) of the imaging system. Alternatively, if $A * G$ is a δ-function (an ideal PSF), then, for any source distribution, equation (3) reduces to

$$S' = S + B * G . \tag{4}$$

We see here that, with such a PSF, this procedure can reproduce the original distribution. The detector background has, however, added a spatially distributed statistical noise to the resulting image.

Since the postprocessing array (G) is derived directly from the mask pattern (A), the requirement that $A * G$ be a δ-function provides the basis for the choice of an appropriate mask pattern. One class of pattern which satisfies this criterion is the *uniformly redundant array* (URA) of Fenimore and Cannon (1978). The mathematical properties and physical implementation of URA mask patterns are thoroughly discussed in Fenimore (1978) and Fenimore and Cannon (1978). The postprocessing function, based on the balanced correlation method (Fenimore and Cannon 1978), is given by

$$\begin{aligned} G(i, j) &= 1 \quad \text{if } A(i, j) = 1 \\ G(i, j) &= -\rho/(1 - \rho) \quad \text{if } A(i, j) = 0 , \end{aligned} \tag{5}$$

where ρ is the fraction of open elements in the mask pattern. (An alternative definition of G is given by Fenimore 1978.) It has been shown, both theoretically and experimentally (Fenimore 1978; Fenimore *et al.* 1979), that URA patterns permit the accurate and unambiguous reconstruction of a source distribution.

A major concern when using a coded-aperture imaging system is the presence of nonuniform background rates within the photon detection plane. Background nonuniformities may arise for a variety of reasons. Contributing factors may include, for example, variations in relative shielding across the detection plane, variations in relative gain, or intrinsic differences among the individual detectors (in the case of a discrete-element array). Such nonuniformities, or background systematics, introduce nonstatistical noise into the reproduced image via the background term of equation (4). (One can think of this in terms of a fixed noise pattern within the field of view.) In many cases, the resulting image degradation cannot be tolerated and therefore some method of eliminating, or at least reducing, the effects of these background systematics is required. We have developed two alternative procedures for dealing with this problem. Both approaches depend on the assumption that the *relative* background rates do not vary in time. The first approach incorporates the use of an *antimask*, which is identical to the mask except that the opaque and transparent elements have been interchanged. This interchange of mask elements recreates the same image noise pattern resulting from the systematics, but it does so with opposite polarity. Therefore, summing together images taken with the mask and antimask eliminates any systematic image noise. The viability of this technique has been previously demonstrated in a series of laboratory imaging tests. (McConnell *et al.* 1982). However, the difficulty of mechanically implementing the antimask scheme on the present UNH balloon gondola has led to the development of an alternative approach which involves the correction of the detector count rates based on the measured relative background rates. This approach is discussed in more detail in § V.

III. INSTRUMENT DESCRIPTION

The University of New Hampshire Directional Gamma-Ray Telescope (DGT) is a balloon-borne experiment which utilizes a coded-aperture mask to image celestial photons over the energy range 160 keV to 9.3 MeV (McConnell *et al.* 1983; Dunphy *et al.* 1987). The DGT instrument is shown schematically in Figure 1. The detection plane consists of a 35-element array of bismuth germanate ($Bi_4Ge_3O_{12}$ or BGO) scintillation crystals actively shielded from below by 10 cm of NaI Polyscin™ and on the sides by 7.5 cm of NaI. The entire anticoincidence well defines a forward geometric aperture of $\sim 120°$ FWHM. Each BGO element is a right-circular cylinder 5.1 cm in diameter by 2 cm thick. BGO was chosen in preference to NaI for the detection plane because of its higher sensitivity per unit volume. For example, the full energy peak efficiency of a single BGO detector element is approximately 17% at 2.6 MeV as opposed to approximately 3% for a NaI crystal of equal size or 2%–3% for a 38 cm^3 Ge detector. The detector array is continuously gain-stabilized using four-gated ^{60}Co calibration sources in a manner directly analogous to that used on the *SMM* gamma-ray spectrometer (Gleske and Forrest 1980). The energy resolution of the gain-stabilized array is measured to be 19% at 0.662 MeV.

The coded mask of the DGT is positioned 84 cm above the detection plane and has outside dimensions 72.8 cm by 50.4 cm. Each opaque element of the mask is composed of a 5.6 cm by 5.6 cm block of lead, of thickness 1.9 cm. Such a thickness is sufficient to attenuate 97% of the photon flux at 0.5 MeV and 60% at 2.6 MeV. The pattern of mask elements is based on a 5 × 7 URA pattern. A single image obtained with the DGT imaging system consists of 35 pixel elements, each representing an area of 3°.8 × 3°.8. The fully coded field of view is 15°.2 × 22°.8. In practice, a source image is composed of a large number of these single images accumulated over the observation period and summed together within some common coordinate system.

Two important aspects of this experiment are worth emphasizing. First, the imaging capability makes the spatial isolation of the source emission a relatively simple task. This eliminates possible contamination of a source spectrum by nearby sources—a problem often encountered in past γ-ray astronomy experiments. Second, background changes due to varying environmental conditions (such as atmospheric depth, rigidity,

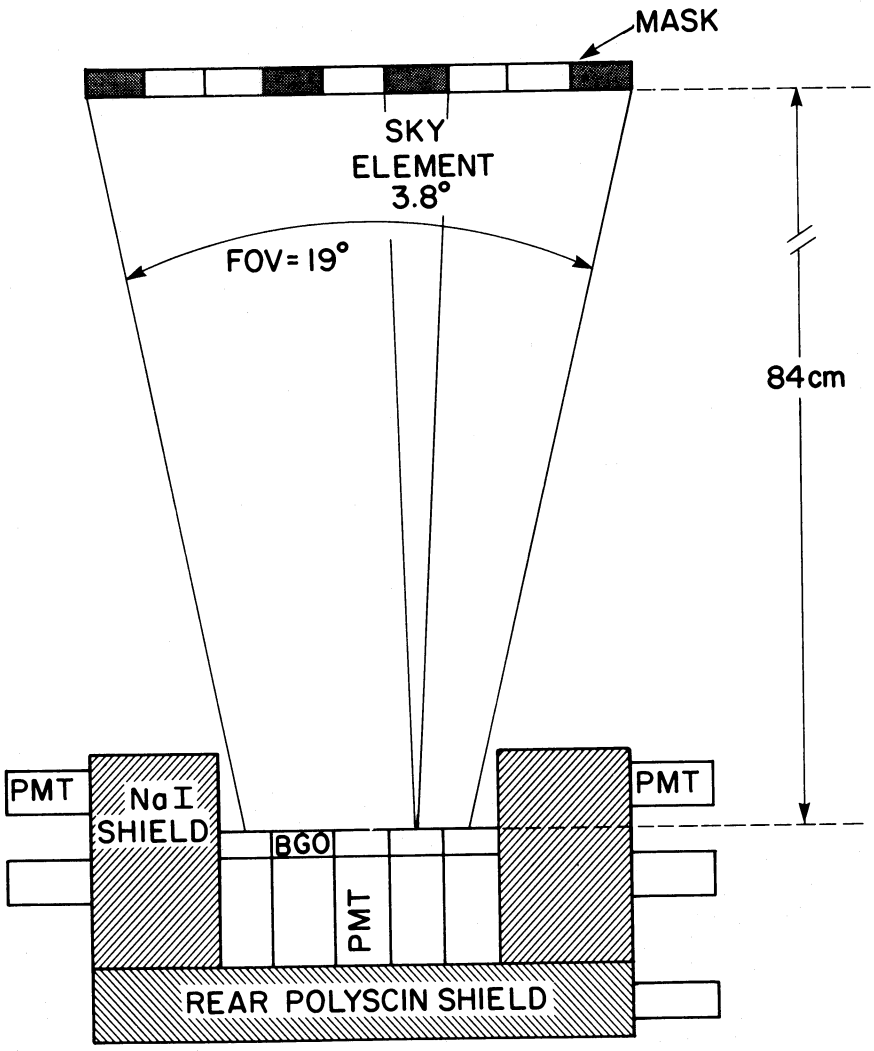

FIG. 1.—Cross sectional view of the Directional Gamma-Ray Telescope (DGT)

etc.) create a time variation in the average detector background. The nature of the coded-aperture process (i.e., simultaneous source-background measurement) is such that the influence of these variations on the imaging results is negligible. This greatly reduces possible sources of error due to temporal variations in the detector background rate.

IV. OBSERVATIONS

The DGT balloon payload was launched from Palestine, Texas, at 14:25 UT on 1984 October 1, reaching a mean float altitude of ~ 3 g cm^{-2} at 17:00 UT. The payload remained at float for ~ 30 hr until termination at 22:35 UT on October 2. Imaging observations of a number of sky regions were made; these observations were centered on the Crab Nebula/pulsar, Cygnus X-1/X-3, NGC 4151, 2CG 135+1, SS 433, and 3C 273. All measurements were performed using a *drift scan* technique in which the source was allowed to drift through several image elements within the field of view. The pointing information from the experiment was verified periodically during the flight using a two-axis solar sensor.

The experiment performed well throughout most of the flight. However, during the first 4 hr at float, a high voltage anomaly produced a change in the threshold of two side segments of the anticoincidence shield. Data taken during this period have been excluded from the present analysis. In general, the BGO detectors showed better than 2% gain stability throughout the flight. Strong background lines at 0.511 MeV, due to atmospheric electron-positron annihilation, and at 1.46 MeV, due to the natural radionuclide ^{40}K, permitted the application of postflight gain corrections to the data. This resulted in an effective overall gain stability of better than 1% for the entire array.

The region of the Crab was observed on 1984 October 2 from 7:30 UT to 10:00 UT and again from 12:30 UT to 15:00 UT, yielding a total source exposure of 3.41×10^6 cm^2 s at 511 keV. Based on measurements at other wavelengths (Pelling *et al.* 1987), we expect the spatial extent of the Crab Nebula to be less than 1′ in the energy range covered by the present observations. Since this size is negligible relative to the DGT's pixel size of 3°.8, we can, in the context of this experiment, consider the Crab Nebula a point source of radiation. This fact, coupled with its fairly stable, well-measured continuum spectrum, makes the Crab an excellent target for evaluating the imaging and spectral measurement capabilities of the DGT.

V. DATA ANALYSIS AND RESULTS

In order to minimize the effects of the background systematics, we have utilized the following approach. The relative background rate of each detector can be quantified by the ratio of that detector's background rate relative to the average rate of the entire array. More specifically,

$$\epsilon_i = B_i/B_{\rm ave} , \tag{6}$$

where ϵ_i is the *systematics correction factor* for the ith detector, B_i the background rate for the ith detector, and $B_{\rm ave} = \sum B_i/N$, the average rate per detector within the array. In practice, the background data used to derive the correction factors are obtained when there are no strong sources in the field of view. These data are accumulated over a period of many hours without taking into account the variations in detector aspect. The large opening aperture of the DGT ($\sim 120°$ FWHM) makes it impractical to eliminate the possibility of weak-source contributions to this measurement. However, due to the drift scan method of observation which was employed, any source counts which are detected during this accumulation period are distributed randomly throughout the detection plane and therefore constitute a nearly uniform DC level. Furthermore, given that the source-to-background ratios for celestial γ-ray sources in this energy range are less than 2%, we can, to first order, neglect the effects of any source contribution to the measurement of the background systematics.

During the actual source observations, the correction factors are used to correct the integrated response of the detector array prior to image extraction (i.e., the correlation defined by eq. [3]). If P_i represents the accumulated response of the ith detector, the modified response (P_i') is given by

$$P_i' = P_i/\epsilon_i . \tag{7}$$

The images produced using the modified detector response (i.e., the P_i') are dominated by statistical, rather than systematics, noise. It should be noted that this process modifies both the background count average value and the source count sum in a given detector. The important quantity, however, is the sum of the source counts within the *entire* array. This sum remains unchanged, since the average value of the ϵ_i is one. We have determined that the maximum possible deviation in the measured source intensity for a single corrected image is not more than 1.5%. Since the composite image for a given source observation is composed of a large number of such images (see below), this effect is reduced even further and therefore has been neglected in the final analysis. As mentioned earlier, the effectiveness of this procedure relies on the assumption that the background systematics, in terms of the ϵ_i, are independent of time. A detailed analysis using the complete flight data base indicates that the systematics are indeed constant to a statistical level of approximately 0.1% of the background for any given energy range. (A detailed description of the observed systematics and this correction procedure may be found in Dunphy *et al.* 1987.)

During a typical source observation, a large number of corrected images are produced. Using the present Crab data set, for example, 236 such images have been created. Each individual image (representing, on the average, ~ 60 s of instrumental livetime) is corrected for relevant observational parameters (such as average pointing direction and balloon location), broken down into 0°.95 × 0°.95 image elements and then transformed into a common *skymap* coordinate frame based on celestial coordinates. The smaller image elements permit a more accurate transformation of the image into the coordinate frame. Once transformed into the skymap frame, the images are then summed together in order to create a composite image of the observed sky region.

The efficacy of this correction procedure is dramatically demonstrated in Figure 2. Here we show a pair of images of the Crab region, one processed with the systematics corrections and one without. Each image covers the (200–600) keV energy range. Without the corrections, the Crab is completely lost in the nonstatistical image noise, but the correction procedure succeeds in reproducing the source at the 10.6 σ level.

A contour map of the total composite image of the Crab region, covering the energy range of (200–600) keV, is shown in Figure 3. (This corresponds to the same data as those displayed in Fig. 2*b*.) It is important to note that the contour map represents the number of reproduced γ-ray events per 0°.95 image element, i.e., the true γ-ray fluence folded through the imaging

1987ApJ...321..543M

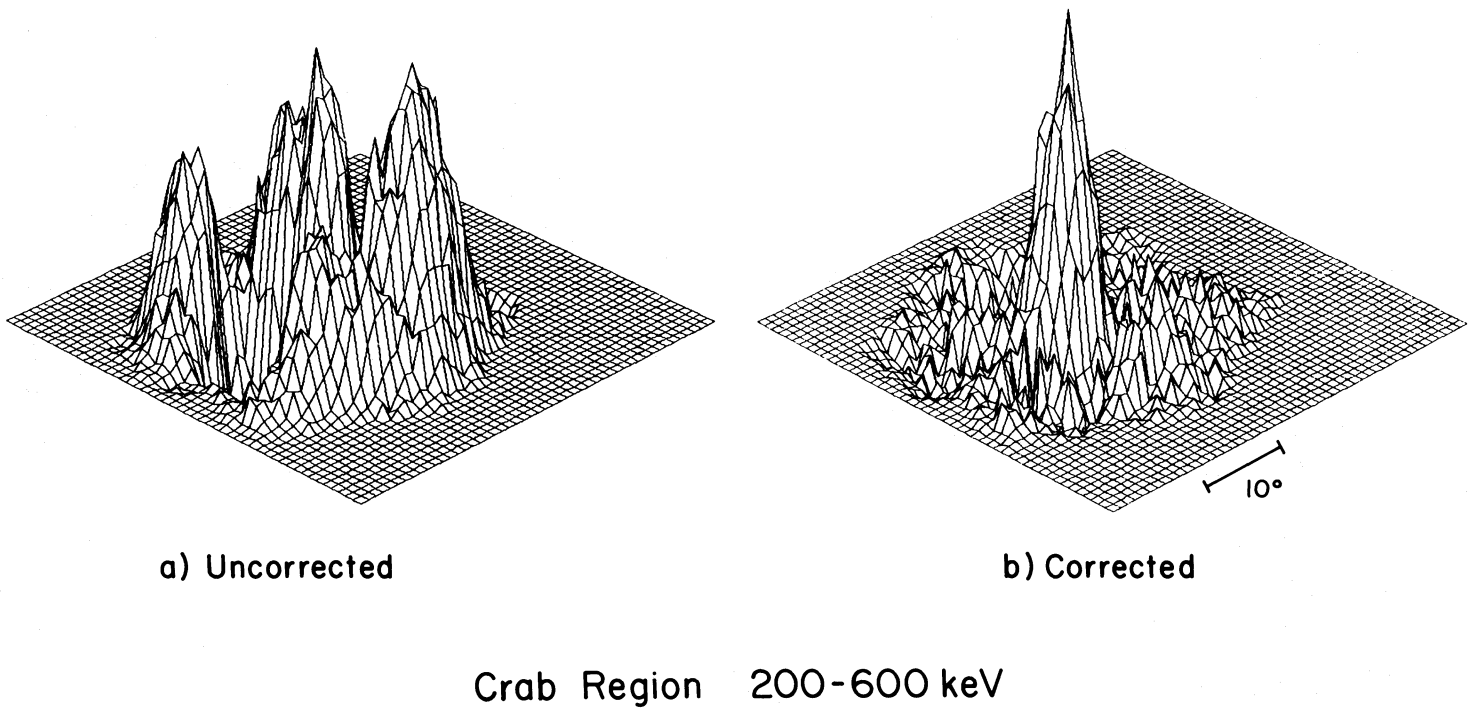

FIG. 2.—Two images of the Crab region, illustrating the efficacy of the background systematics correction. (Each view represents the reproduced γ-ray intensity.) Figs. 2*a* and 2*b* show the uncorrected and corrected data, respectively. The amplitude of the peak in Fig. 2*b* corresponds to a significance in the detected flux of 10.6 σ. The total source observation livetime was 12,842 s.

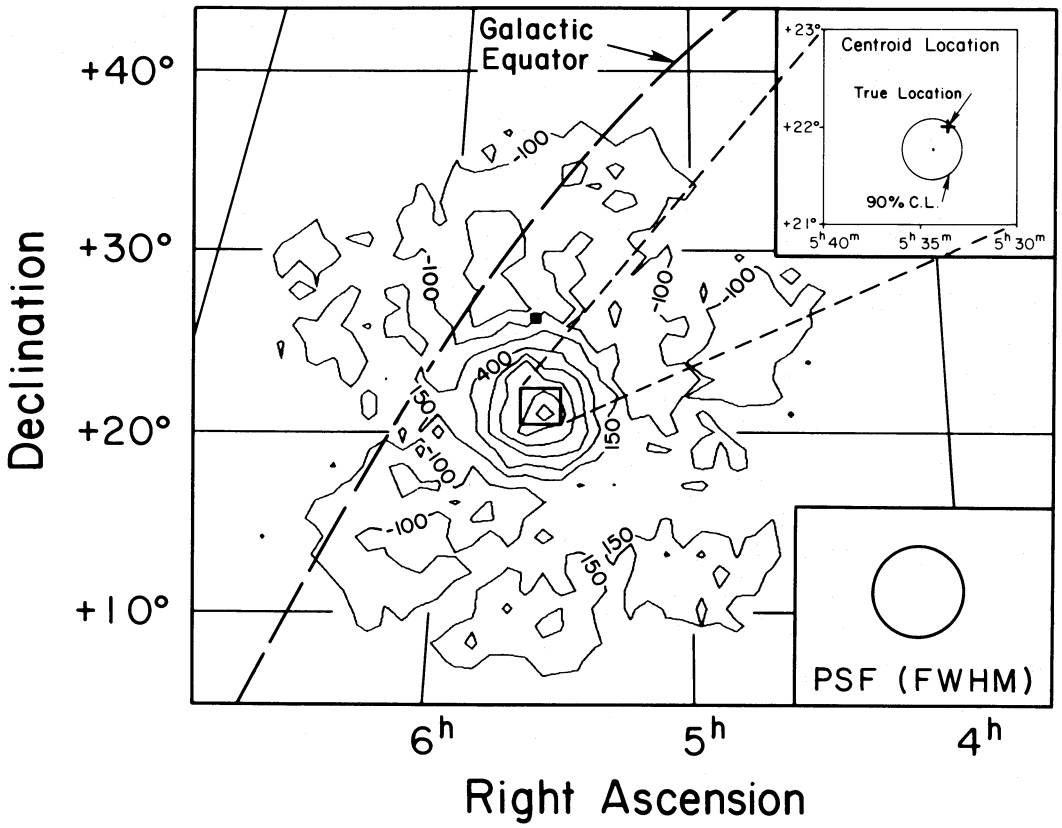

FIG. 3.—Reproduced intensity contour of the Crab region γ-ray emission (200–600 keV). The contour values represent the reproduced number of γ-ray events per ($0.^{\circ}95 \times 0.^{\circ}95$) image pixel. Due to the nature of the image reproduction process, the average nonsource image element lies at a level of approximately -80. The data are consistent with a single point source located at the Crab. The inset shows the 90% confidence contour for the measured peak location (as measured in the 160 keV to 1 MeV range). For comparison the true position of the Crab is also shown. The location of A0535+26 is shown by the small square.

PSF. Similar data, integrated over the energy range 160 keV to 1 MeV, have been used to directly measure the inflight PSF of the imaging system. For the (160 keV–1 MeV) composite image, it is found that the PSF is well represented in the skymap coordinate frame by a five-parameter Gaussian function. The five parameters are the peak location (μ_x and μ_y), the peak width (σ_x and σ_y), and the peak area (I). The measured width of the PSF (average of σ_x and σ_y) leads to a FWHM of $4.^{\circ}8 \pm 0.^{\circ}4$. (Instabilities in the orientation system broaden the measured PSF beyond the basic $3.^{\circ}8$ element size by $\sim 25\%$.)

The ability to measure the position of a celestial γ-ray source depends primarily on the measured source statistics and the width of the instrumental PSF. Since the PSF can be approximated by a Gaussian, the estimated location error can be written as

$$\sigma_{\rm loc} \approx \sigma_{\rm PSF}/n_{\sigma} , \qquad (8)$$

where $\sigma_{\rm loc}$ is the error on the source location, $\sigma_{\rm PSF}$ refers to the width of the measured PSF, and n_{σ} is the significance of the measurement in terms of the number of standard deviations of the source signal above the mean background level. The inset of Figure 3 shows the 90% confidence contour for the Crab centroid location, based on an analysis of the (160 keV to 1 MeV) imaging data using a *bootstrap sampling* procedure (Simpson and Mayer-Hasselwander 1986). At the 68% (1 σ) confidence level, the source is located to an accuracy of $\pm 12'$. From equation (8) and the measured values of $\sigma_{\rm PSF} = 2^{\circ}$ and $n_{\sigma} = 10.4$, we expect an error of $\pm 11.'5$, in good agreement with the measured error. The true Crab location (also noted in Fig. 3) is offset from the measured location by an amount which is consistent with our estimated uncertainty in the pointing system of $\pm 30'$.

In order to construct a spectrum of the Crab, we have produced a total of seven separate composite images, each covering a different energy interval. The total energy range covered by these images is 160 keV to 9.3 MeV. From each image, the total number of observed source counts can be determined by fitting the measured PSF to the imaging response of the source, with the width and centroid location of the PSF (i.e., σ_x, σ_y, μ_x, and μ_y) kept fixed during the fitting procedure. The actual values of the PSF were determined from fitting the total imaging data for the energy interval 160 keV to 1 MeV. This range was chosen so as to provide the best available statistics. Errors on the derived source intensity are determined using a bootstrap sampling analysis. The total number of source and background events for each energy interval is given in Table 1. This process allows us to construct an energy-loss spectrum (i.e., number of detected source counts as a function of energy) for the Crab. This energy-loss spectrum is then compared to a library of response spectra previously generated by folding

TABLE 1

SOURCE AND BACKGROUND COUNT RATES FOR EACH OF THE ENERGY INTERVALS CONSIDERED IN THE PRESENT ANALYSIS

Energy (MeV)	Background Counts s^{-1}	Source Counts s^{-1}
0.160–0.200.....	93.64	0.96 ± 0.15
0.200–0.250.....	85.54	1.26 ± 0.17
0.250–0.300.....	61.68	0.67 ± 0.12
0.300–0.400.....	87.11	0.63 ± 0.14
0.400–0.800.....	187.29	1.00 ± 0.22
0.800–2.000.....	131.89	0.61 ± 0.21
2.000–9.310.....	61.76	0.09 ± 0.12

model source spectra through the instrument's response function. (The analysis also incorporates the energy-dependent and time-dependent atmospheric attenuation during the observation period.) In this fashion, the best-fit parameters for a given source model can be derived, along with the allowable parameter ranges. The resulting best-fit power-law spectrum of the Crab (incident on the top of the atmosphere) is given by $5.1 \times 10^{-3} E(\mathrm{MeV})^{-1.88}$ photons cm^{-2} s^{-1} MeV^{-1} (with a reduced χ^2 of 1.5 for 5 degrees of freedom). This spectrum, along with the 90% confidence contour for the power-law parameters, is shown in Figure 4.

We have also performed a search of the Crab data for reported line emission at 405 keV and 1050 keV (Owens, Myers, and Thompson 1985). The search was accomplished by producing composite images integrated over three energy ranges for each line energy—one range centered on the line location and one on either side of the line location. The flux of the candidate line was determined by comparing counts in the center bin with the average source continuum on either side of the central bin. Each energy range corresponds to 1.2 times the FWHM of the detector energy resolution at the line energy. (Jacobson *et al.* [1975] have shown that this is the optimum bin width with which to detect a line in the presence of a background continuum.) The measured residuals are statistically consistent with zero flux, allowing us to place 3 σ upper limits on line emission at 405 keV and 1050 keV of 3.2×10^{-3} and 1.9×10^{-3} photons cm^{-2} s^{-1}, respectively. These values may be compared with those reported by Owens, Myers, and Thompson (1985) of $(7.3 \pm 2.1) \times 10^{-3}$ and $(2.0 \pm 0.5) \times 10^{-2}$ photons cm^{-2} s^{-1}, respectively. A search for line structure down to a flux level of $\sim 10^{-3}$ photons cm^{-2} s^{-1} is in progress, over the energy range 160 keV to ~ 9 MeV.

In addition to the Crab Nebula, there are two other sources of interest which were within the field of view during the Crab observation. The first such source is the flaring binary X-ray source A0535+26, whose angular separation from the Crab is only 4°.4. The DGT measurements show no evidence for this source. Upper limits on the flux level from A0535+26 have been derived using a procedure which fits both the Crab and A0535+26 simultaneously. The results are shown in Figure 5. We can also note that the spatial resolution of the DGT, in conjunction with our null flux measurement, allows us to con-

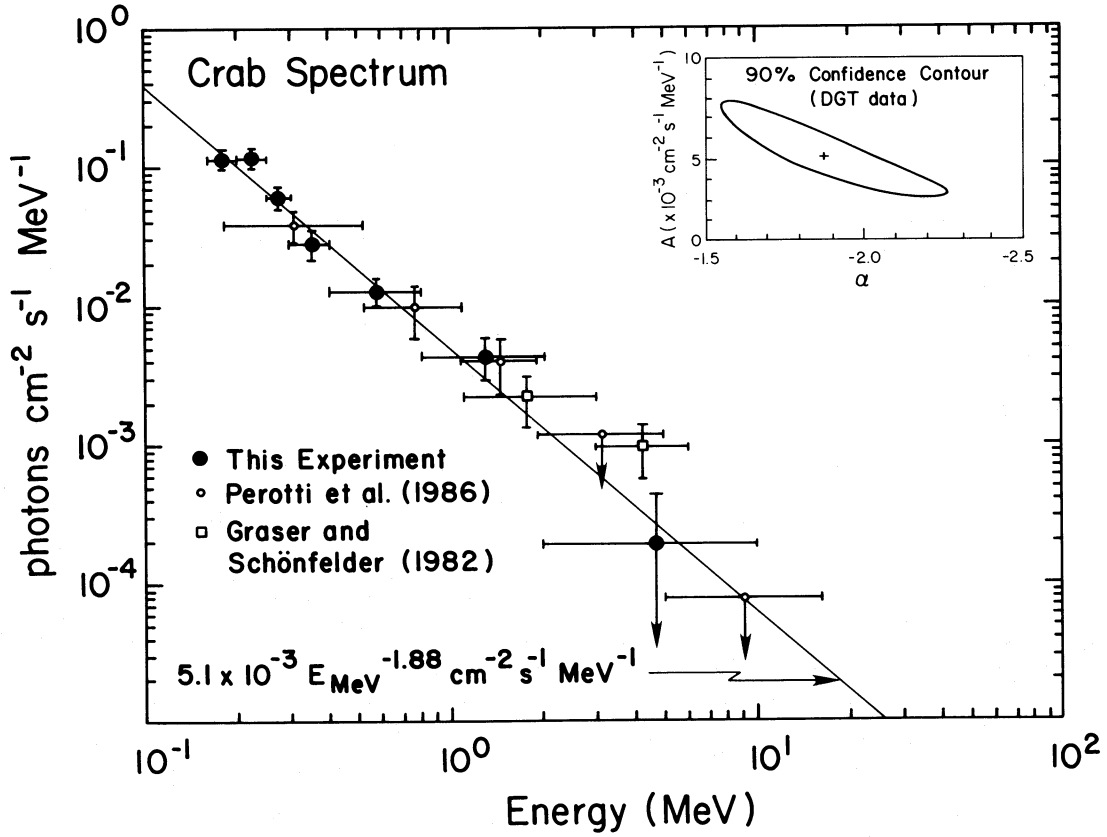

FIG. 4.—The total Crab photon spectrum as measured by the DGT. The solid line through the data points represents the best fit to the DGT data using a power law of the form $dN(E)/dE = AE^{-\alpha}$. The inset shows the 90% confidence contour for the joint estimation of the two parameters A and α. For comparison, other representative data points are shown.

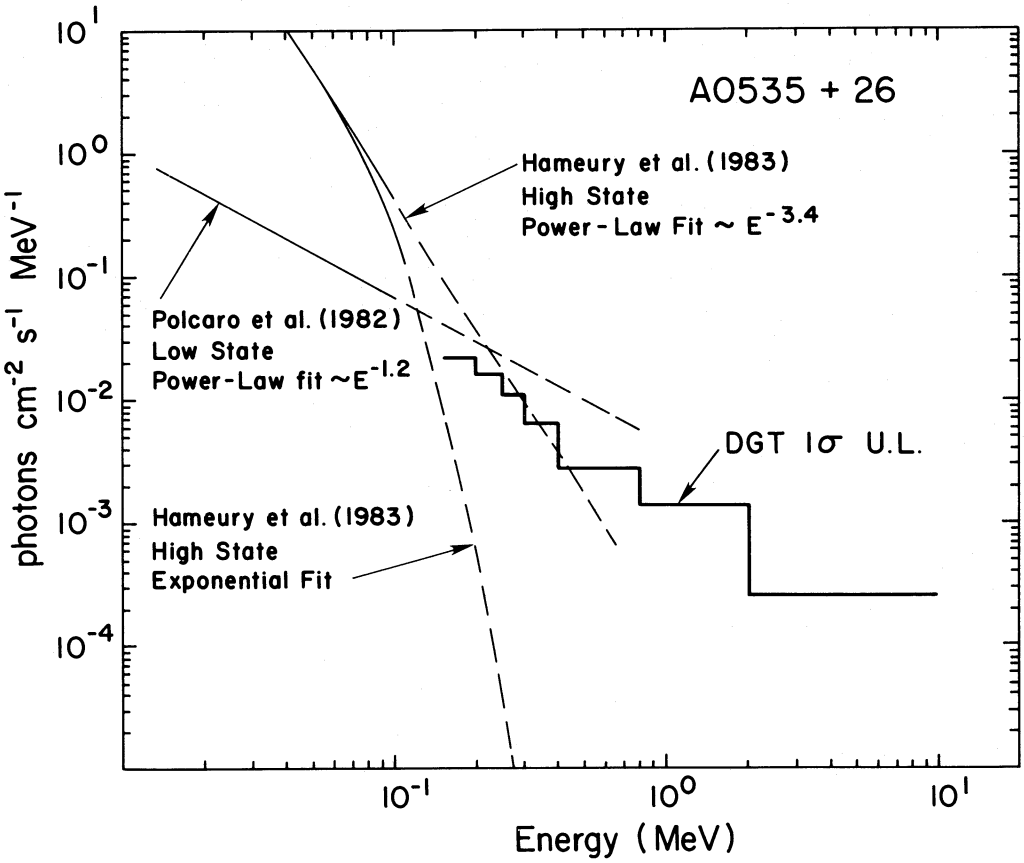

FIG. 5.—The upper limit flux levels from A0535+26 as derived from the DGT imaging data. Lower energy X-ray measurements (<100 keV), along with their extrapolations to higher energies, are shown for comparison.

clude that A0535+26 does not contribute significantly (i.e., <10%) to the measured Crab spectrum.

The second source of interest is the spatially extended flux reported by Graser and Schönfelder (1982) in the 1 to 10 MeV energy range. This emission, located near the Crab, was observed to lie along the Galactic equator (Galactic longitude range, $l = 160°$–$197°$) with a FWHM scale height relative to the Galactic plane of approximately 4°. The DGT image of this region shows no evidence for such emission. The imaging data have therefore been used to set upper limits on the diffuse flux. The emission has been modeled using a series of point sources distributed along 15° of the Galactic plane ($l = 175°$–$190°$), thus approximating the distribution observed by Graser and Schönfelder (1982). The results of this analysis are displayed in Figure 6.

VI. DISCUSSION

Our measurement of the Crab photon spectrum is consistent with a power law extending to at least 9 MeV. For example, we find no evidence for any excess emission over the power law at energies greater than 1 MeV, as had been reported by some previous observers (Baker *et al.* 1973; Gruber and Ling 1977). Gruber and Ling (1977) suggested that this emission might be due to the nearby source A0535+26. The null results obtained here for A0535+26 indicate that this source does not contribute to the observed Crab spectrum at MeV energies. Ayre *et al.* (1983) suggested that the narrow-line emission observed at 1049.8 keV might account for the observed "MeV excess." However, as discussed above, there is no evidence for any such line emission in the present data set.

Past observations of A0535+26 (see Hameury *et al.* [1983] and references therein) suggest a 111 day period between successive "high" states, at which times it can attain a flux level 5 times that of the Crab at 20 keV. Based on the 111 day period and extrapolating from the high-state observations of 1980 October 5 (Hameury *et al.* 1983; Frontera *et al.* 1982), we find that the DGT observation took place only 14 days after the time of predicted peak activity. As shown in Figure 5, the DGT upper limits are inconsistent with power-law extrapolations of X-ray data obtained in both the low state (Polcaro *et al.* 1982) and the high state (Hameury *et al.* 1983). This result supports the interpretation of the A0535+26 photon spectrum as being best described by either an exponential (e.g., Hameury *et al.* 1983) or a thermal (e.g., Frontera *et al.* 1982) spectrum with no measurable emission at MeV energies.

The DGT upper limits for the diffuse anticenter emission (Fig. 6) lie slightly above the data points of Graser and Schönfelder (1983), which are based on the interstellar electron spectrum given by Lebrun *et al.* (1982).

VII. CONCLUSIONS

We have successfully demonstrated, for the first time, the ability of the coded-aperture technique to image celestial γ-ray photons by imaging the region of the Crab Nebula/pulsar in

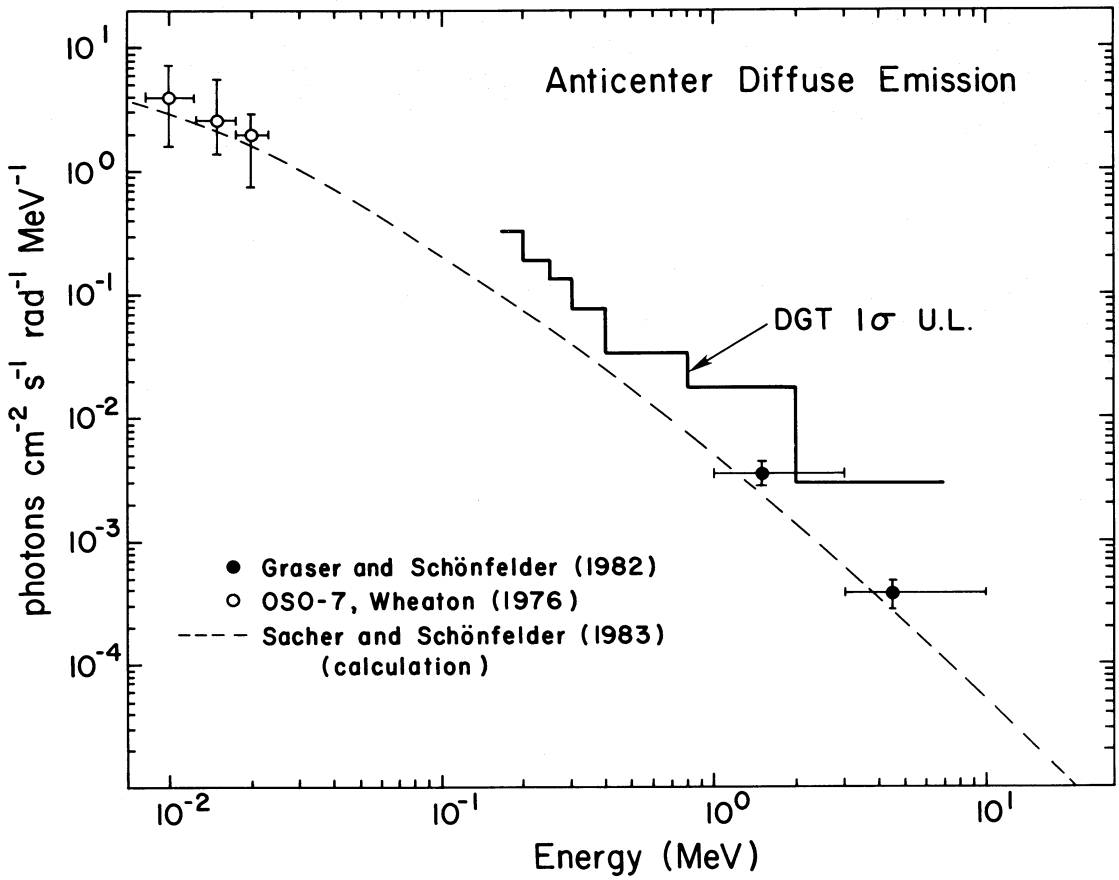

FIG. 6.—The upper limit flux levels from the Galactic anticenter diffuse emission (Galactic longitude, $l = 175°$–$190°$) as derived from the DGT imaging data. The measurements of Wheaton (1976) for $l = 240°$ and Graser and Schönfelder (1982) for $l = 160°$ to $197°$ are shown for comparison. The calculations of Sacher and Schönfelder (1983) for the emission due to an $E^{-2.8}$ interstellar electron spectrum (Lebrun *et al.* 1982) are also shown.

the energy range of 160 keV to 9.3 MeV. We have also shown that the problem of background systematics can be effectively dealt with by using a simple and relatively straightforward correction procedure. The present results allow us to conclude that the coded-aperture procedure is a viable approach for imaging not only point sources of radiation, but also extended sources of emission. In addition to providing an assessment of the DGT's imaging capabilities, the data have been used to simultaneously measure the Crab's photon spectrum. The spectral results are consistent with a power-law spectrum. The Crab spectral results allow us to derive upper limits on the flux levels of line emission at 405 keV and 1050 keV. Finally, the imaging nature of the experiment (coupled with its large field of view) has also permitted the derivation of upper limits on the flux from the X-ray binary source A0535+26 and diffuse galactic emission from the anticenter region.

We would like to thank the staff of the National Scientific Balloon Facility for a successful balloon flight. Special thanks go to J. Googins for his support throughout the project. Indulis Gleske and M. Lauritzen were responsible for much of the design and development of the electronics. Thanks also to D. Bhattacharya and M. Popeki for their contributions to the data analysis and to M. M. Chupp, K. Dowd, and S. Cote for final preparation of the manuscript. This work was supported by NASA grant NGL 30-002-021.

REFERENCES

Ables, J. G. 1968, *Proc. Astr. Soc. Australia*, **4**, 172.
Ayre, C. A., Bhat, P. N., Ma, Y. Q., Myers, R. M., and Thompson M. G. 1983, *M.N.R.A.S.*, **205**, 285.
Baker, R. E., Lovett, R. R., Orford, K. J., and Ramsden, D. 1973, *Nature Phys. Sci.*, **245**, 18.
Cook, W. R., Finger, M., Prince, T. A., and Stone, E. C. 1983, *IEEE Trans. Nucl. Sci.*, **NS-31**, No. 1, 771.
Dicke, R. H. 1968, *Ap. J. (Letters)*, **153**, L101.
Dunphy, P. P., McConnell, M. L., Chupp, E. L., Forrest, D. J., and Owens, A. 1987, in preparation.
Fenimore, E. E. 1978, *Appl. Optics.*, **17**, 3562.
Fenimore, E. E., and Cannon, T. M. 1978, *Appl. Optics*, **17**, 337.
Fenimore, E. E., Cannon, T. M., Van Hulsteyn, D. B., and Lee, P. 1979, *Appl. Optics*, **18**, 945.
Frontera, F., Dal Fiume, D., Dusi, W., Morelli, E., Spada, G., and Ventura, G. 1982, in *Accreting Neutron Stars*, ed. W. Brinkman and J. Trümper (Garching: MPI), p. 112.
Gleske, I. U., and Forrest, D. J. 1980, *IEEE Trans. Nucl. Sci.*, **NS-27**, 313.
Graser, U., and Schönfelder, V. 1982, *Ap. J.*, **263**, 677.
Gruber, D. E., and Ling, J. C. 1977, *Ap. J.*, **213**, 802.
Hameury, J. M., Boclet, D., Durouchoux, Ph., Cline, T. L., Paciesas, W. S., Teegarden, B. J., Tueller, J., and Haymes, R. C. 1983, *Ap. J.*, **270**, 144.
Jacobson, A. S., Bishop, R. J., Culp, G. W., Mahoney, W. A., and Willett, J. B. 1975, *Nucl. Instr. Meth.*, **127**, 115.
Jenkins, T. L., Frye, G. M., Owens, A., Carter, J. N., and Ramsden, D. 1984, *Nucl. Instr. Meth.*, **221**, 278.
Lebrun, F., *et al.* 1982, *Astr. Ap.*, **107**, 390.
Leventhal, M., MacCallum, C. J., and Watts, A. C. 1977, *Nature*, **266**, 696.
Ling, J. C., Mahoney, W. A., Willett, J. B., and Jacobson, A. S. 1979, *Ap. J.*, **231**, 896.
Manchanda, R. K., Bazzano, A., La Padula, D. C., Polcaro, V. F., and Ubertini, P. 1982, *Ap. J.*, **252**, 172.
McConnell, M. L., Dunphy, P. P., Forrest, D. J., and Chupp, E. L. 1983, in *Adv. Space Res.*, Vol. **3**, No. 4, 105.

McConnell, M. L., Forrest, D. J., Chupp, E. L., and Dunphy, P. P. 1982, *IEEE Trans. Nucl. Sci.*, **NS-29**, 155.
Owens, A., Myers, R. M., and Thompson, M. G. 1985, *Proc. 19th Internat. Cosmic Ray Conf.*, La Jolla, **1**, 145.
Pelling, M. R., Paciesas, W. S., Peterson, L. E., Makishima, K., Oda, M., Ogawara, Y., and Miyamoto, S. 1987, *Ap. J.*, **319**, 416.
Perotti, F., *et al.* 1986, *Ap. J.*, **300**, 297.
Polcaro, V. F., Bazzano, A., La Padula, C., Ubertini, P., Vialetto, G., and Manchanda, R. K. 1982, in *Accreting Neutron Stars*, ed. W. Brinkman and J. Trümper (Garching: MPI), p. 117.
Proctor, R. J., Skinner, G. K., and Willmore, A. P. 1978, *M.N.R.A.S.*, **185**, 745.
Ramaty, R., and Lingenfelter, R. E. 1982, *Ann. Rev. Nucl. Part. Sci.*, **32**, 235.
Sacher, W., and Schönfelder, V. 1983, *Space Sci. Rev.*, **36**, 249.
Simpson, G., and Mayer-Hasselwander, H. 1986, *Astr. Ap.*, **162**, 340.
Skinner, G. K., *et al.* 1986, *Bull. A.A.S.*, **18**, 675.
Strickman, M. S., Kurfess, J. D., and Johnson, W. N. 1982, *Ap. J.* (*Letters*), **253**, L23.
Watanabe, H. 1985, *Ap. Space Sci.*, **111**, 157.
Wheaton, W. A. 1976, Thesis, University of California at San Diego.
Yoshimori, M., Watanabe, H., Okudaira, K., Hirasima, Y., and Murakami, H. 1979, *Australian J. Phys.*, **32**, 375.

E. L. CHUPP, P. P. DUNPHY, D. J. FORREST, M. L. McCONNELL, and A. OWENS: Physics Department, DeMeritt Hall, University of New Hampshire, Durham, NH 03824